A Brucite-Like Mixed-Valent Cluster Capped by [MnIIIp-tBu-calix[4]arene]− Moieties

chemistry

MDPI

Communication

A Brucite-Like Mixed-Valent Cluster Capped by [Mn^{III}*p*-^{t}Bu-calix[4]arene]$^{-}$ Moieties

Marco Coletta [1], Maria A. Palacios [1,†], Euan K. Brechin [1,*] and Scott J. Dalgarno [2,*]

1 EaStCHEM School of Chemistry, University of Edinburgh, Joseph Black Building, David Brewster Road, Edinburgh EH9 3FJ, UK; marco.coletta@ed.ac.uk (M.C.); mpalacios@ugr.es (M.A.P.)
2 Institute of Chemical Sciences, School of Engineering and Physical Sciences, Heriot-Watt University, Riccarton, Edinburgh EH14 4AS, UK
* Correspondence: E.Brechin@ed.ac.uk (E.K.B.); S.J.Dalgarno@hw.ac.uk (S.J.D.); Tel.: +44-131-650-7545 (E.K.B.); +44-131-451-8025 (S.J.D.)
† Current address: Departamento de Química Inorgánica, Facultad de Ciencias, Universidad de Granada, 18071 Granada, Spain.

Received: 30 March 2020; Accepted: 8 April 2020; Published: 9 April 2020

Abstract: *p*-^{t}Bu-calix[4]arene (H_4TBC[4]) has proven to be an incredibly versatile ligand for the synthesis of 3*d*- and 3*d*/4*f*- clusters, in particular those containing mixed-valent Mn ions. These are of interest to the magnetochemist for the diversity of magnetic behaviours that can be shown, along with a huge variety of nuclearities and topologies accessible, which allow one to outline magneto-structural correlations and a quantitative understanding of their properties. This contribution reports the synthesis, analysis and magnetic properties of a Brucite-like Mn-oxo/hydroxo octanuclear fragment encapsulated within/capped by four [Mn^{III}-TBC[4]]$^{-}$ moieties. A diol coligand in the reaction mixture plays a seemingly important role in determining the outcome, though it is not incorporated in the final structure.

Keywords: calixarenes; coordination clusters; manganese; molecular magnetism

1. Introduction

Manganese continues to play a prominent role in the chemistry of 3*d* transition metals, owing to its significance across a breadth of research areas, including bioinorganic [1] and biomedicinal chemistry [2], catalysis [3], nanomaterials [4], spectroscopy [5], and molecular magnetism [6]. In the latter category, the ability of the Mn ion to exist in a variety of stable oxidation states (II-IV) allows for the construction of polymetallic cluster compounds exhibiting a variety of interesting magnetic behaviours, including the stabilization of large spin ground states [7], the slow relaxation of magnetization [8], spin frustration [9], vibrational coherences [10], and enhanced magnetocaloric effects [11]. A key component in understanding the physical properties of all Mn-based molecular magnets is the construction of large families of related compounds so that structure-magnetism relationships can be quantitatively rationalised, and this requires the careful design and exploitation of specific organic bridging ligands.

We have been exploring the coordination chemistry of calix[*n*]arenes (C[*n*]s) with Mn (as well as other metals), as these molecules hold the potential to isolate coordination clusters in the solid state in various different ways, for example, by exploiting the wedge shape of *p*-^{t}Bu-calix[4]arene (H_4TBC[4]). As can be seen from the acetonitrile (CH_3CN) solvate of H_4TBC[4] (Figure 1a) [12], the shape of the building block exerts strong influence over assembly and typically results in antiparallel bilayer formation in the solid state. The hydrophobic cavities are offset in this case and are occupied by acetonitrile of crystallization, though the same phenomenon is also observed for other solvates such

as dmf [13]. With respect to cluster formation, *p*-^{t}Bu-calix[4]arene (H_4TBC[4]) has proven to be a particularly versatile platform for the synthesis of a wide range of different topologies, with nuclearities reaching up to fourteen [13–16]. A recurring structural theme we have noticed in this work is that the $[Mn^{III}TBC[4]]^{-}$ moieties act as bridges to metal ions within the cluster through their phenolate groups (Figure 1b), but also as polyhedral capping units (Figure 1c) [17]. The latter suggests that these can be used to encapsulate small metal-oxo-hyroxo fragments growing in 2- or 3-dimensions. Thia, sulfonyl and sulfinyl calix[4]arenes have also been employed in this way, though they give access to markedly different topologies due to the presence of donor atoms at the bridge positions [18–23]. In all cases, new species isolated with methylene- or heteroatom-bridged calix[4]arenes would be of particular interest to magnetochemists researching topological spin frustration [24]. Herein, we discuss the synthesis, structure and magnetic behaviour of a mixed-valent $[Mn^{III}_8Mn^{II}_4]$ species built with TBC[4], the core metallic skeleton of which is related to the hydroxide-based mineral Brucite.

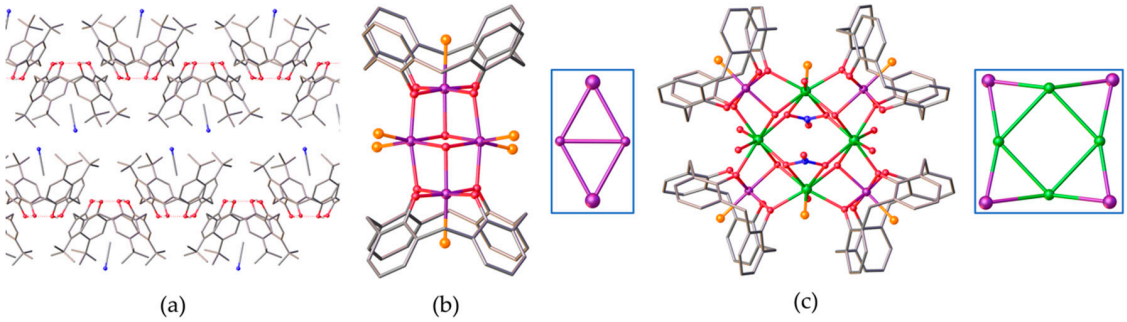

Figure 1. (**a**) Section of the extended structure found in the CH_3CN solvate of H_4TBC[4], showing the antiparallel bi-layer assembly and offset head-to-head arrangement of the host cavities [12]. (**b**) Partial single crystal X-ray structure of a mixed-valence TBC[4]-supported manganese cluster containing a butterfly-like $[Mn^{III}_2Mn^{II}_2(OH)_2]$ core [13]. Mn^{III} ions occupy the tetraphenolato pocket of the TBC[4] and act as capping units (shown as larger spheres in the inset diagram). (**c**) Partial single crystal X-ray structure of a C[4]-supported 3*d*-4*f* cluster topology that can be isolated with a range of lanthanides [14]. Analogous capping behaviour to that found in (**b**) is also observed here and is represented by the larger spheres in the inset diagram. Colour code: Mn^{III}—purple; Ln^{III}—green; O—red; C—grey; N—blue; ligated solvent—orange. ^{t}Bu groups, hydrogen atoms, and solvent of crystallization omitted for clarity.

2. Results and Discussion

2.1. Synthesis and Structural Studies

Reaction of H_4TBC[4] with $MnCl_2{\cdot}6H_2O$, H_2bd (1,4-butanediol), $[NH_4]ClO_4$, and NEt_3 in a mixture of CH_3CN and dmf, followed by vapour diffusion of diethyl ether into the mother liquor, afforded single crystals suitable for X-ray diffraction of formula $[Mn^{III}_8Mn^{II}_4(\mu_4\text{-}O)_2(\mu_3\text{-}OH)_6(\mu\text{-}OH)_4(\mu\text{-}Cl)_2(TBC[4])_4(dmf)_8(H_2O)_4(CH_3CN)_2]{\cdot}2dmf{\cdot}6CH_3CN$ (**1**, Figure 2, please also see Appendix A). The crystals were found to be in a triclinic cell, and structure solution was carried out in the space group *P*-1, with the asymmetric unit (ASU) comprising half of the cluster (Mn1–Mn6, Figure 3). Before moving to the structural description of **1**, it is interesting to note that inspection of Figure 2 shows that 1,4-butanediol is not incorporated in the prevailing structure. Our original intention was to form a heteroleptic TBC[4]-diol cage, and although 1,4-butanediol is not incorporated, its presence in the reaction mixture is required for **1** to form. Indeed, analogous experiments in the absence of diol result in the formation of the well-known TBC[4]-supported $[Mn^{III}_2Mn^{II}_2]$ cluster topology shown in Figure 1B; this particular cluster can be isolated quantitatively in under 1 h, further indicating that the diol plays a crucial role in the formation of **1**.

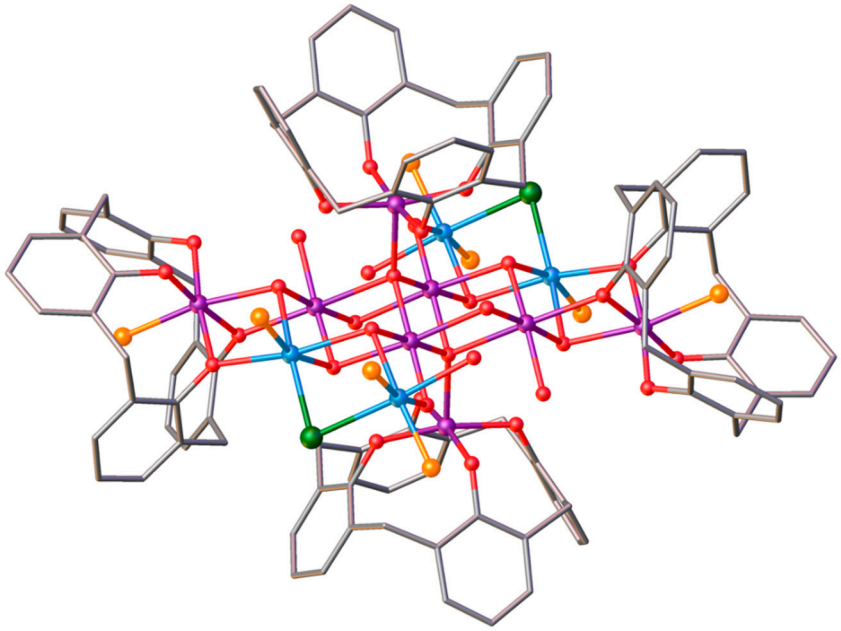

Figure 2. Partial single crystal X-ray structure of **1**. Colour code: Mn^{III}—purple; Mn^{II}—pale blue; O—red; C—grey; Cl—green; ligated dmf—orange sphere. ^{t}Bu groups, hydrogen atoms, solvent of crystallization and atoms other than oxygen of ligated dmf are omitted for clarity.

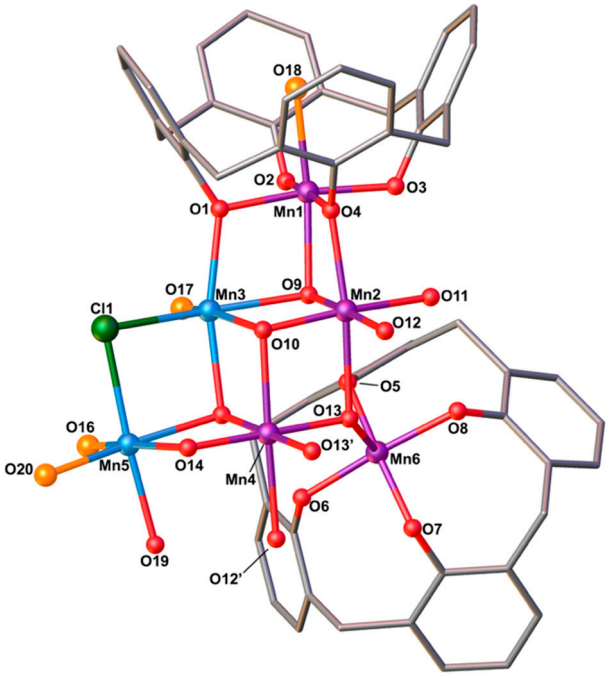

Figure 3. Partial single crystal X-ray structure of **1** showing the asymmetric unit with selected labels shown. Colour code: Mn^{III}—purple; Mn^{II}—pale blue; O—red; C—grey; Cl—green; dmf—orange. ^{t}Bu groups, hydrogen atoms, and solvent of crystallization omitted for clarity. Two s.e. atoms (O12′ and O13′) are included in order to show the octahedral coordination sphere around Mn4.

The central metal–oxygen core of **1** describes a near-planar, mixed-valent $[Mn^{III}_6Mn^{II}_4(\mu_4\text{-}O)_2(\mu_3\text{-}OH)_6(\mu\text{-}OH)_4(Cl)_2]$ sheet-like structure (Figures 2 and 4). The Mn^{III} ions in **1** (Mn1, Mn2, Mn4, and symmetry equivalent, s.e.) are easily distinguished through the presence of coparallel Jahn-Teller (JT) axes, oriented approximately 40° from the plane of the metal ions. The two Cl ions (Cl1 and s.e.) bridge between neighbouring Mn^{II} ions (Mn3-Cl-Mn5 and s.e.,

86.21°). Mn1 (and s.e.) is bound in a TBC[4] lower-rim tetraphenolato pocket (Mn1-O1-4, with bond distances in the range of 1.882(2)–1.973(2) Å), with its distorted octahedral geometry completed by a ligated dmf molecule residing within the TBC[4] cavity (Mn1–O18, 2.271(3) Å), and a μ_3-OH (Mn1–O9, 2.216(2) Å) that also bridges Mn2 and Mn3 (Mn2–O9, 1.931(2) Å and Mn3–O9, 2.209(3) Å). The remaining Mn^{III} ion (Mn6 and s.e.) is also bound within a TBC[4] lower-rim tetraphenolato pocket (Mn6-O5-8, with bond distances in the range of 1.930(2)–1.948(2) Å) sitting above/below the [Mn_{10}] plane (Figure 2), bonded to Mn2 and Mn4 (and s.e.) through a μ_4-O^{2-} ion (Mn6–O13, 2.144(2) Å). Each of these O-atoms is H-bonded to a bridging hydroxide in the [Mn_{10}] plane (O···O, 2.643–2.870 Å).

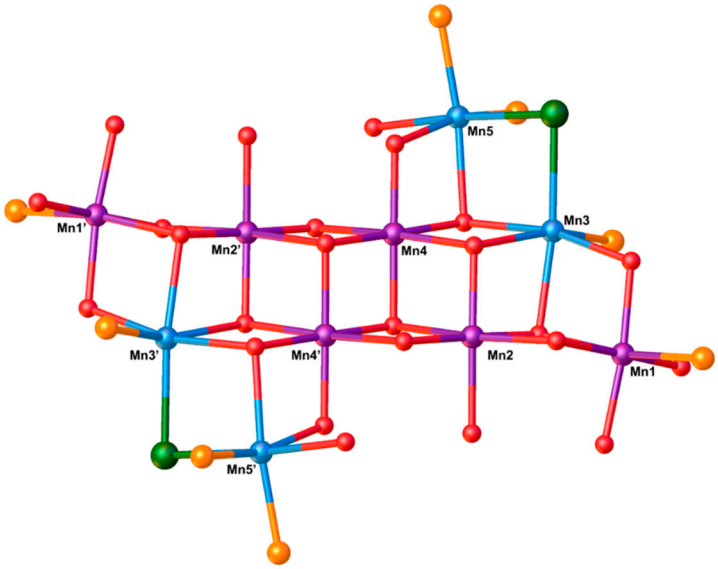

Figure 4. The near-planar, mixed-valent [$Mn^{III}_6Mn^{II}_4(\mu_4\text{-}O)_2(\mu_3\text{-}OH)_6(\mu\text{-}OH)_4(Cl)_2$] sheet-like structure at the core of complex **1**. Colour code: Mn^{III}—purple; Mn^{II}—pale blue; O – red; Cl—green; dmf—orange. Carbon, nitrogen and hydrogen atoms, as well as solvent of crystallization omitted for clarity.

Interestingly, Mn6 (and s.e.) is formally five-coordinate and in square-pyramidal geometry (Figure 3), with the CH_3CN molecule occupying the TBC[4] cavity and interacting with the Ph rings through CH···π interactions. We have observed such behaviour in other TBC[4]-supported Mn cages [25], and this is also reminiscent of the host-guest chemistry found in the CH_3CN solvate of TBC[4] (Figure 1a) [12]. The preference of the TBC[4] ligands to host Mn^{III} ions over Mn^{II} ions in **1** is entirely consistent with our previously published empirical binding rules for this ligand [17].

One of the goals behind our use of C[*n*]s in cluster synthesis is to isolate or 'dilute' these species in the solid state. This has been achieved efficiently in the formation of **1**, with TBC[4]s protecting the cluster core (Figure 5). The closest intermolecular interactions found between s.e. of **1** in the extended structure occur between Cl ions at a Cl···Cl distance of ~3.3 Å, and between dmf molecules at an N···O distance of ~3.6 Å, directing chains of [Mn_{12}] cages along the *a*-axis of the cell. Inspection of Figure 5 and comparison with Figure 1A shows similar assembly behaviours despite the fact that the overall shape of **1** is markedly different to that of the parent H_4TBC[4]. The 'coating' of **1** with [Mn^{III}TBC[4]]$^-$ capping moieties results in head-to-head packing dominated by the calixarenes. This is another common structural trend that is emerging as this work progresses, another example being that trigonal planar enneanuclear [Cu^{II}_9] clusters adapt to display similar packing behaviour in sheets, even though the clusters are unable to form the typical bi-layers. Interestingly, the metal–oxygen core present in **1** (Figure 4) is reminiscent of a portion of the Brucite ([$Mg(OH)_2$]) lattice, and is similar to that observed in [$Mn_{6–12}$] "rods" built with the tripodal alcohol ligands H_3thme (1,1,1-tris(hydroxymethyl)ethane) and H_3tmp (1,1,1-tris(hydroxymethyl)propane) [26], and to the [$Mn^{III}_6Mn^{II}_4$] "planar discs" built with the ligands 2-amino-2-methyl-1,3-propanediol ($ampH_2$) and 2-amino-2-ethyl-1,3-propanediol ($aepH_2$) [27].

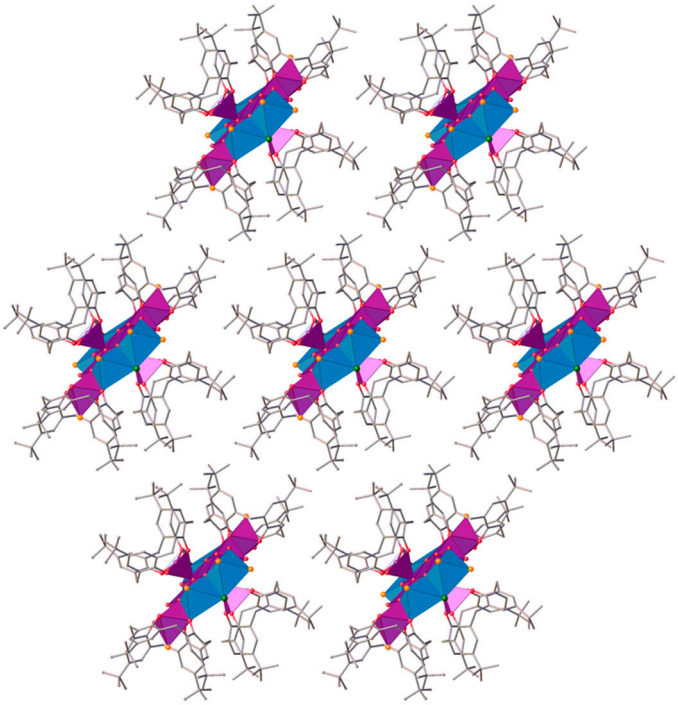

Figure 5. Extended structure of **1** looking down the *a*-axis. Packing of neighbouring clusters is dominated by TBC[4]s, which mimic head-to-head dimer assembly akin to that shown for the CH_3CN solvate of H_4TBC[4] in Figure 1a [12]. Colour code: Mn^{III}—purple polyhedra; Mn^{II}—pale blue polyhedra; O—red; C—grey; hydrogen atoms, solvent of crystallization and ligated solvent omitted for clarity.

2.2. Magnetic Behaviour

Magnetic susceptibility (χ_M) data were measured on a powdered, restrained crystalline sample of **1** under a 0.1 T dc field in the T = 5–300 K temperature range. The temperature dependence of the χ_MT product is shown in Figure 6. At room temperature, the χ_MT value of 40.82 cm^3 K mol^{-1} is close to the Curie constant expected for eight Mn^{III} and four Mn^{II} ions, assuming a *g*-value of 2.00 (41.5 cm^3 K mol^{-1}). The χ_MT value remains approximately constant as the temperature is decreased until ~150 K, where it starts to decrease, reaching a minimum value of 13.27 cm^3 K mol^{-1} at 5 K. This behaviour is indicative of the presence of predominantly weak antiferromagnetic interactions between the constituent metal ions. A fit of the $1/\chi_M$ versus T data to the Curie–Weiss law afforded the Weiss constant, $\theta = -10$ K. Magnetization measurements, performed in fields between 0.5–7 T (Figure 7), are in agreement with this observation, showing M increasing in a near linear like fashion with H, indicative of the field-induced population of low-lying excited states with larger magnetic moments. Previous magneto-structural correlations in alkoxide-bridged Mn^{III} dimers in which the JT axes are coparallel, as seen in the central [Mn_{10}] planar core (Figure 4), predict borderline and weak ferro- or antiferromagnetic exchange interactions, as observed [28]. No signals were observed in ac susceptibility measurements for data collected in the T = 1.8–10 K temperature range in frequencies up to 1500 Hz.

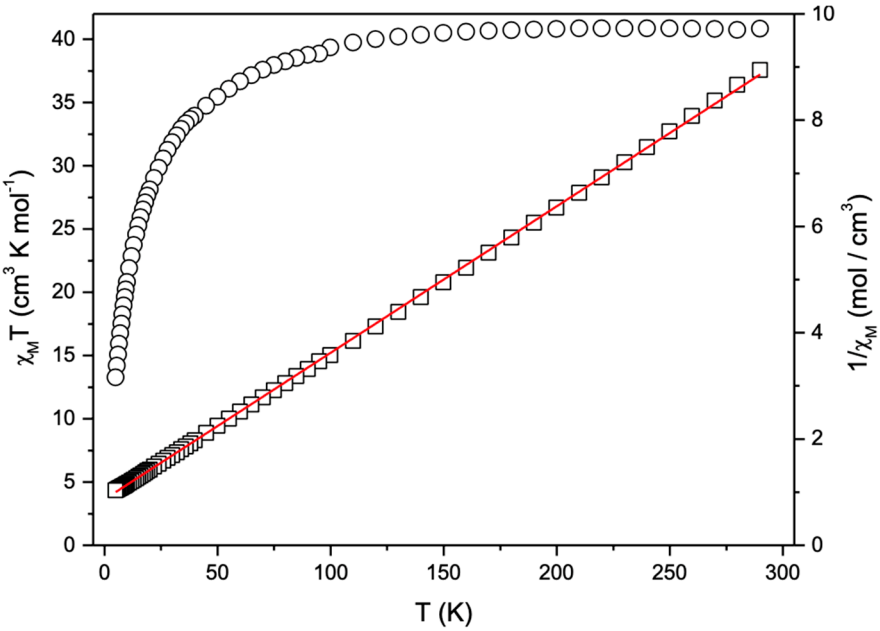

Figure 6. Plot of $\chi_M T$ vs T (o) and $1/\chi_M$ vs T (□) in the range T = 5–300 K in an applied field of 0.1 T. The red line is a fit of the Curie–Weiss law. See text for details.

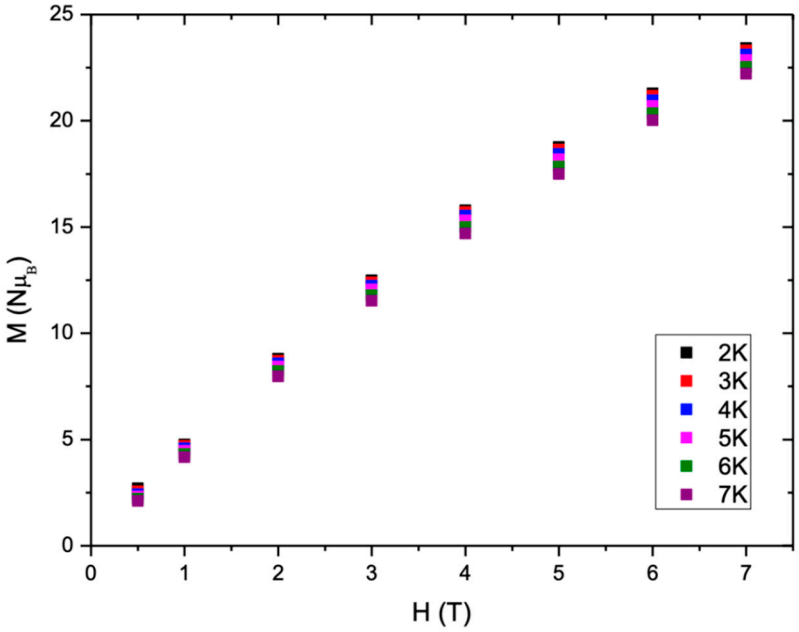

Figure 7. Field dependence of the magnetization (M) measured in the range T = 2–7 K and H = 0.5–7.0 T.

3. Conclusions

The reaction between $MnCl_2{\cdot}6H_2O$, H_4TBC[4], H_2bd, $[NH_4][ClO_4]$ and NEt_3 in CH_3CN / dmf affords the dodecametallic, mixed-valent cluster $[Mn^{III}_8Mn^{II}_4(\mu_4\text{-}O)_2(\mu_3\text{-}OH)_6(\mu\text{-}OH)_4(\mu\text{-}Cl)_2(TBC[4])_4(dmf)_8(H_2O)_4(CH_3CN)_2]$. The structure describes a central, near-planer Mn-oxo-hydroxo moiety, reminiscent of the Brucite lattice, encapsulated by $[Mn^{III}\text{-}TBC[4]]^-$ moieties. Magnetic susceptibility and magnetization measurements reveal dominant and weak antiferromagnetic exchange interactions between the metal centres.

Somewhat surprisingly, 1,4-butanediol is a crucial component required for the formation of **1** despite the fact that it is not incorporated in the resulting cluster. Absence of this key reactant affords the previously reported mixed-valence TBC[4]-supported Mn-butterfly cluster, suggesting that this

chelate plays a crucial role in (possibly hindering) cluster formation and producing a significantly higher nuclearity species in the process; the TBC[4]-supported Mn-butterfly cluster (Figure 1b) can be formed rapidly in approximately 15 min, and quantitatively precipitates from solution within an hour. The development reported here suggests that the use of other potential coligands with similar chemical make-up may offer the possibility to access/isolate other large, discrete high-nuclearity species. Results from this study will be reported in due course and will ideally shed additional light on the important role of such non-innocent reactants.

Author Contributions: Conceptualization, S.J.D. and E.K.B.; methodology, M.A.P.; formal analysis, M.A.P., M.C.; writing, M.C., E.K.B. and S.J.D.; visualization, M.C., S.J.D.; funding acquisition, S.J.D., E.K.B. All authors have read and agreed to the published version of the manuscript.

Funding: This research was funded by the EPSRC through grant reference numbers EP/I03255X/1 and EP/I031421/1.

Conflicts of Interest: The authors declare no conflict of interest.

Appendix A

$MnCl_2{\cdot}4H_2O$ (99 mg, 0.5 mmol, Sigma Aldrich, UK), H_4TBC[4] (97 mg, 0.15 mmol, Sigma Aldrich, UK) and NH_4ClO_4 (140 mg, 1.2 mmol, Sigma Aldrich, UK) were dissolved in a mixture of dmf (10 mL, Fisher Scientific, UK) and CH_3CN (10 mL, Fisher Scientific, UK). 1,4 butanediol (90 mg, 1 mmol, Sigma Aldrich, UK) was then added with stirring. After five minutes, NEt_3 (0.42 mL, 3 mmol, Sigma Aldrich, UK) was added dropwise and the reaction mixture stirred for two hours. X-ray quality crystals were obtained after 3 days in ~20% yield following filtration of the mother liquor with subsequent diffusion of diethyl ether (or hexane) into the resulting solution. Elemental analysis: found (calc. %) for $C_{222}H_{320}Cl_2Mn_{12}N_{18}O_{42}$: C 57.61 (57.43), H 6.94 (6.95), N 5.35 (5.43). Crystal Data (CCDC 1993320): $C_{204}H_{288}Cl_2Mn_{12}N_{10}O_{40}$ (M =4250.61 g/mol): triclinic, space group P-1 (no. 2), a = 16.144(16) Å, b = 19.437(19) Å, c = 22.33(2) Å, α = 110.119(15)°, β = 104.06(2)°, γ = 90.752(15)°, V = 6347(11) Å^3, Z = 1, T = 100(2) K, μ(MoKα) = 0.656 mm^{-1}, *Dcalc* = 1.112 g/cm^3, 98657 reflections measured (3.342° ≤ 2Θ ≤ 52.744°), 25871 unique (R_{int} = 0.0328, R_{sigma} = 0.0396), which were used in all calculations. The final R_1 was 0.0564 (I > 2σ(I)) and wR_2 was 0.1810 (all data). Magnetic properties were determined using a MPMS-XL SQUID magnetometer (Quantum Design Inc., San Diego, CA, USA) for direct current (dc) and alternating current (ac) measurements. The powdered microcrystalline sample was immobilised in eicosane. Experimental dc data were recorded at 0.1 T in the temperature range 5.0–300 K and at 2.0–7.0 K in the field range 0.5–7.0 T. Experimental ac data were collected in the temperature range 1.8–10 K and frequency range 0–1500 Hz using an amplitude of B_{ac} = 3 G. All data were corrected for the sample holder contributions and intrinsic diamagnetic contributions that were determined from Pascal's constants.

References

1. Ferreira, K.N.; Iverson, T.M.; Maghlaoui, K.; Barber, J.; Iwata, S. Architecture of the photosynthetic oxygen-evolving center. *Science* **2004**, *303*, 1831–1838. [CrossRef]
2. Ali, B.; Iqbal, M.A. Coordination complexes of manganese and their biomedical applications. *ChemistrySelect* **2017**, *2*, 1586–1604. [CrossRef]
3. Sampson, M.D.; Nguyen, A.D.; Grice, K.A.; Moore, C.E.; Rheingold, A.L.; Kubiak, C.P. Manganese catalysts with bulky bipyridine ligands for the electrocatalytic reduction of carbon dioxide: Eliminating dimerization and altering catalysis. *J. Am. Chem. Soc.* **2014**, *136*, 5460–5471. [CrossRef] [PubMed]
4. Diehl, S.J.; Lehmann, K.J.; Gaa, J.; McGill, S.; Hoffmann, V.; Georgi, M. MR Imaging of pancreatic lesions. Comparison of manganese-DPDP and gadolinium chelate. *Invest. Radiol.* **1999**, *34*, 589–595. [CrossRef] [PubMed]
5. Davis, K.M.; Palenik, M.C.; Yan, L.; Smith, P.F.; Seidler, G.T.; Dismukes, G.C.; Pushkar, N. X-ray Emission Spectroscopy of Mn Coordination Complexes towards Interpreting the Electronic Structure of the Oxygen Evolving Complex of Photosystem II. *J. Phys. Chem. C* **2016**, *120*, 3326–3333. [CrossRef]

6. Sessoli, R.; Boulon, M.-E.; Caneschi, A.; Mannini, M.; Poggini, L.; Wilhelm, F.; Rogalev, A. Strong magneto-chiral dichroism in a paramagnetic molecular helix observed by hard X-ray. *Nat. Phys.* **2015**, *11*, 69–74. [CrossRef]
7. Shiga, T.; Nojiri, H.; Oshio, H. A Ferromagnetically Coupled Octanuclear Manganese(III) Cluster: A Single-Molecule Magnet with a Spin Ground State of S = 16. *Inorg. Chem.* **2020**. [CrossRef]
8. Sessoli, R.; Gatteschi, D.; Caneschi, A.; Novak, M.A. Magnetic bistability in a metal-ion cluster. *Nature* **1993**, *365*, 141–143. [CrossRef]
9. McCusker, J.K.; Schmitt, E.A.; Hendrickson, D.N. High Spin Inorganic Clusters: Spin Frustration in Polynuclear Manganese and Iron Complexes. In *Magnetic Molecular Materials*; Gatteschi, D., Kahn, O., Miller, J.S., Palacio, F., Eds.; NATO ASI Series (Series E: Applied Sciences); Springer: Dordrecht, The Netherlands, 1991; Volume 198.
10. Liedy, F.; Eng, J.; McNab, R.; Inglis, R.; Penfold, T.J.; Brechin, E.K.; Johansson, J.O. Vibrational coherences in manganese single-molecule magnets after ultrafast photoexcitation. *Nat. Chem.* **2020**. [CrossRef]
11. Evangelisti, M.; Brechin, E.K. Recipes for enhanced molecular cooling. *Dalton Trans.* **2010**, *39*, 4672–4676. [CrossRef]
12. Asfari, F.; Bilyk, A.; Bond, C.; Harrowfield, J.M.; Koutsantonis, G.A.; Langkeek, N.; Mocerino, M.; Skelton, B.W.; Sovolev, A.N.; Strano, S.; et al. Factors influencing solvent adduct formation by calixarenes in the solid state. *Org. Biomol. Chem.* **2004**, *2*, 387–396. [CrossRef] [PubMed]
13. Karotsis, G.; Teat, S.J.; Wernsdorfer, W.; Piligkos, S.; Dalgarno, S.J.; Brechin, E.K. Calix[4]arene-based single-molecule magnest. *Angew. Chem. Int. Ed.* **2009**, *48*, 8285–8288. [CrossRef] [PubMed]
14. Karotsis, G.; Evangelisti, M.; Dalgarno, S.J.; Brechin, E.K. A calix[4]arene 3d/4f magnetic cooler. *Angew. Chem. Int. Ed.* **2009**, *48*, 9928–9931. [CrossRef] [PubMed]
15. Taylor, S.M.; McIntosh, R.D.; Piligkos, S.; Dalgarno, S.J.; Brechin, E.K. Calixarene-supported clusters: Employment of complementary cluster ligands for the construction of a ferromagnetic [Mn5] cage. *Chem. Commun.* **2012**, *48*, 11190–11192. [CrossRef]
16. McLellan, R.; Palacios, M.A.; Sanz, S.; Brechin, E.K.; Dalgarno, S.J. Importance of Steric Influences in the Construction of Multicomponent Hybrid Polymetallic Clusters. *Inorg. Chem.* **2017**, *56*, 10044–10053. [CrossRef]
17. Coletta, M.; Brechin, E.K.; Dalgarno, S.J. Structural trends in calix[4]arene-supported cluster chemistry. In *Calixarenes and Beyond*; Neri, P., Sessler, J.L., Wang, M.-X., Eds.; Springer International Publishing: Cham, Switzerland, 2016; Chapter 25; pp. 671–689.
18. Sone, T.; Ohba, Y.; Moriya, K.; Kumada, H.; Kazuski, I. Synthesis and properties of sulfur-bridged analogs of *p-tert*-Butylcalix[4]arene. *Tetrahedron* **1997**, *53*, 10689–10698. [CrossRef]
19. Mislin, G.; Graf, E.; Hosseini, M.W.; Bilyk, A.; Hall, A.K.; Harrowfield, J.M.; Skelton, B.W.; White, A.H. Thiacalixarenes as cluster keepers: Synthesis and structural analysis of a magnetically coupled tetracopper(II) square. *Chem. Commun.* **1999**, 373–374. [CrossRef]
20. Iki, N.; Kabuto, C.; Fukushima, T.; Kumagai, H.; Takeya, H.; Miyanari, S.; Miyashi, T.; Miyano, S. Synthesis of *p-tert*-Butylthiacalix[4]arene and its Inclusion Property. *Tetrahedron* **2000**, *56*, 1437–1443. [CrossRef]
21. Morohashi, N.; Iki, N.; Sugawara, A.; Miyano, S. Selective oxidation of thiacalix[4]arenes to the sulfinyl and sulfonyl counterparts and their complexation abilities toward metal ions as studied by solvent extraction. *Tetrahedron* **2001**, *57*, 5557–5563. [CrossRef]
22. Bi, Y.F.; Du, S.C.; Liao, W.P. Thiacalixarene-based nanoscale polyhedral coordination cages. *Coord. Chem. Rev.* **2014**, *276*, 61–72. [CrossRef]
23. Su, K.Z.; Jiang, F.L.; Qian, J.J.; Chen, L.; Pang, J.D.; Bawaked, S.M.; Mokhtar, M.; A-Thabaiti, S.A.; Hong, M.C. Stepwise Construction of Extra-Large Heterometallic Calixarene-Based Cages. *Inorg. Chem.* **2015**, *54*, 3183–3188. [CrossRef] [PubMed]
24. Schnack, J. Effects of frustration on magnetic molecules: A survey from Olivier Kahn until today. *Dalton Trans.* **2010**, *39*, 4677–4686. [CrossRef] [PubMed]
25. Coletta, M.; Sanz, S.; McCormick, L.J.; Teat, S.J.; Brechin, E.K.; Dalgarno, S.J. The remarkable influence of *N,O*-ligands in the assembly of a bis-calix[4]arene-supported [$Mn^{IV}_2Mn^{III}_{10}Mn^{II}_8$] cluster. *Dalton Trans.* **2017**, *46*, 16807–16811. [CrossRef] [PubMed]

26. Rajaraman, G.; Murugesu, M.; Sañudo, E.C.; Soler, M.; Wernsdorfer, W.; Helliwell, M.; Muryn, C.; Raftery, J.; Teat, S.J.; Christou, G.; et al. A Family of Manganese Rods: Syntheses, Structures, and Magnetic Properties. *J. Am. Chem. Soc.* **2004**, *126*, 15445–15457. [CrossRef] [PubMed]
27. Manoli, M.; Collins, A.; Parsons, S.; Candini, A.; Evangelisti, M.; Brechin, E.K. Mixed-Valent Mn Supertetrahedra and Planar Discs as Enhanced Magnetic Coolers. *J. Am. Chem. Soc.* **2008**, *130*, 11129–11139. [CrossRef]
28. Berg, N.; Rajeshkumar, T.; Taylor, S.M.; Brechin, E.K.; Rajaraman, G.; Jones, L.F. What Controls the Magnetic Interaction in bis-μ-Alkoxo Mn^{III}Dimers? A Combined Experimental and Theoretical Exploration. *Chem. Eur. J.* **2012**, *18*, 5906–5918. [CrossRef]